Three-Sheet Spot Welding of Advanced High-Strength Steels

The weldability of thin, low-carbon steel to two thicker, high-strength steels is studied through factorial experimentation and statistical analysis

C. V. NIELSEN, K. S. FRIIS, W. ZHANG, AND N. BAY

ABSTRACT

The automotive industry has introduced the three-layer weld configuration, which represents new challenges compared to normal two-sheet lap welds. The process is further complicated by introducing high-strength steels in the joint. The present article investigates the weldability of thin, low-carbon steel to two thicker, high-strength steels of high-strength low-alloy (HSLA) 340, DP600, or TRIP700. Factorial experimentation and statistical analysis are used to illustrate how the robustness of the process is affected by the electrode size and is heavily influenced by the protective zinc coating. The weld mechanisms are analyzed numerically and compared with metallographic analyses showing how the primary bonding mechanism between the thin, low-carbon steel sheet and the thicker sheet of high-strength steel is solid-state bonding, whereas the two high-strength steels are joined by melting, forming a weld nugget at their mutual interface. Despite the absence of the typical fusion nugget through the interface between the low-carbon steel and high-strength steel, the weld strengths obtained are acceptable. The failure mechanism in destructive testing is ductile fracture with plug failure.

Introduction

The automotive industry is constantly seeking product and production optimization. Resistance spot welding is a key technology in automotive assembly production. The process is fast and can easily weld many different material combinations that are difficult or even impossible to join by other welding techniques. The development of new, advanced high-strength steels (AHSS) for use in the automotive industry represents new challenges to the resistance welding of these steels. These new steel types are often used in supporting parts of the car and in parts that are designed to absorb the impact of a crash. The parts are typically joined to considerably thinner and softer low-carbon sheet materials that act as the outer panels of the car.

The weldability of different AHSS in two-layer lap joints has been investigated by several authors including the present ones (Refs. 1–5). Problems due to the formation of hard martensite phases during the rapid cooling after welding increase the risk of the joints having brittle fracture. Narrow weld lobes initiated work (Ref. 6), where an insulating adhesive layer is added between the sheets to form a weld bond. The adhesive layer increases the heat and, thereby, the nugget size due to higher contact resistance. Wider weld lobes were shown, but the addition of the adhesive layer complicates the assembly process.

Joining three sheets by resistance spot welding is an increasing trend in automotive assembly. Compared to two-sheet spot welding, joining three sheets is significantly more complicated because of the extra interface introduced. The use of different material combinations and different sheet thicknesses in the three layers complicates the process even further. Spot welding of three low-carbon steel sheets was investigated (Ref. 7), where it was recommended that three-sheet spot welding should be avoided whenever it could be replaced by two spot welds of two sheets. Among the difficulties were coating, varying surface quality, and enhanced alignment problems between three sheets compared to two. Successful welds were made, but it was shown that the three-sheet welds are more sensitive to changing parameters. Lack of confidence in weld quality is also mentioned for spot welding three sheets (Ref. 8), which in industry results in many more welds than actually needed for the required structural performance. In their study, the focus was on the heat development for uncoated and coated low-carbon steels. For these steels, they obtain acceptable weld qualities for three-sheet welding.

When resistance spot welding three sheets, the joint has two sheet-to-sheet interfaces with positions relative to each other and the electrodes depending on the individual sheet thicknesses. If one of the outer sheets is considerably thinner than the other two sheets, the interface between this and the center sheet is located closer to the neighboring electrode than the other interface. In this case, the large heat conduction to the electrode creates an asymmetrical heat distribution causing problems achieving a successful weld. If the heat input is too small, the nugget will not develop in the thinner sheet, and the weld will be unsuccessful. On the other hand, if the heat input is too large, splash is often observed between the two thicker sheets, leading to uncontrollable material removal, loss of strength, and excessive electrode wear. In many cases, this implies unsatisfactory weld strength. Of importance to car manufacturing, spot welding of a thin, low-carbon steel sheet to two thicker, high-strength steels is an example with the above complications.

Innovative solutions to the above type of three-sheet spot welding have been developed (Refs. 9, 10). One solution (Ref. 9) is intelligent control of the electrode force and current levels to ensure nugget formation in both interfaces. Using a high current and low force setting in the beginning of the weld, a nugget is formed in the interface between the thin, low-carbon

KEYWORDS

Low-Carbon Steel
High-Strength Steel
HSLA 340
DP600
TRIP700
Weld Nugget
Plug Failure

C. V. NIELSEN, K. S. FRIIS, and N. BAY (nbay@mek.dtu.dk) *are with the Department of Mechanical Engineering, Technical University of Denmark, Lyngby, Denmark. W. ZHANG is with SWANTEC Software and Engineering ApS, Lyngby, Denmark.*

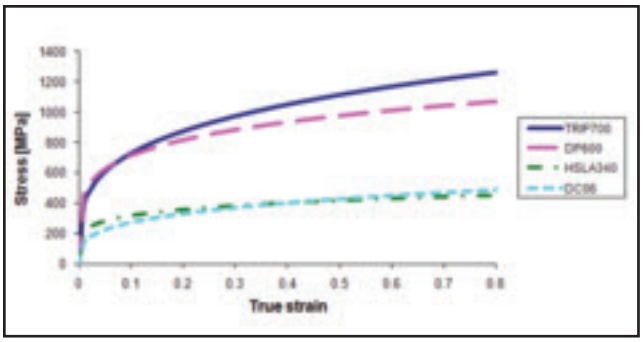

Fig. 1 — Room temperature tensile properties of the applied steels. The curves represent best-fit Hollomon equations of tested data.

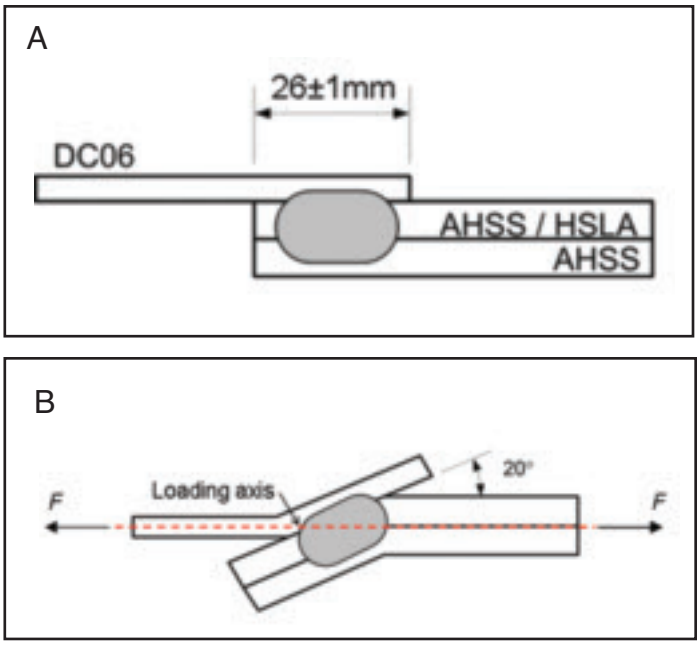

Fig. 2 — Test specimens' alignment; A — During welding; B — before tension shear testing.

sheet and the neighboring thicker high-strength steel. The later part of the weld is performed using relatively lower current and larger force, whereby the nugget forms in the interface between the two thicker high-strength steels. Another solution to the problem is to use a process tape between the electrodes and sheets (Ref. 10). By choosing a proper resistance of the process tape in contact with the thinner low-carbon sheet, it is possible to produce relatively more heat at the interface to the thin sheet. The two methods (Refs. 9, 10) both ease the challenges to this three-sheet combination. However, both methods require advanced equipment available, either variable weld current and force during the weld time, or introduction of process tape around the electrode tip.

It may be difficult to achieve the optimum parameter settings for such a joint and the robustness of the process might be poor and highly influenced by stochastic variations. When welding high-strength steels, the electrode force required to avoid splash is often high due to the high hardness of the steels. However, when spot welding two layers of AHSS with a third layer of soft, low-carbon steel, the latter will typically experience significant electrode indentation due to the high load, which in many cases is unacceptable due to aesthetic reasons.

The present work deals with the weld mechanism and weldability of three-layer spot welding of a thin, low-carbon steel sheet to high-strength low-alloy (HSLA) and AHSS sheets investigating different material combinations. None of the methods (Refs. 9, 10) are applied, such that the present work reflects spot welding with common conventional welding equipment. The objective is to study the influence of the main parameters on weld strength and nugget development in order to improve the understanding of the problems involved in three-sheet spot welding. Factorial experimentation is used to design and analyze the experiments with regard to the weld strength. Furthermore, the nugget size and resulting microstructure have been investigated. The experimental results are compared with a numerical model using the finite element method and experimentally determined material data.

Experimental

Experimental Procedure

Experiments were performed on a TECNA 8105 AC welding machine with a TE-180 weld controller. The electrical system can deliver up to 85 kA with 50 Hz. The actual current was measured using a Rogowski coil together with a precalibrated TECNA-1430 conditioner. The mechanical system is pneumatically driven and can deliver up to 20 kN (4.50 klbf) weld force. The actual load during the welding process was measured continuously using a piezoelectric force transducer. The applied electrodes were Ø20 mm (13⁄16 in.) and Ø16 mm (5⁄8 in.) ISO type B CuCrZr with tip diameters Ø8 mm (5⁄16 in.) and Ø6 mm (1⁄4 in.), respectively. Splash was recorded during welding both visually and by observing any irregular fluctuations in the measured weld force. The materials available for the investigation are listed in Table 1 including sheet thicknesses as well as nominal compositions. They include two types of AHSS (DP600 and TRIP700), a HSLA steel (HSLA 340), and a low-carbon steel (DC06). Figure 1 shows the tensile properties at room temperature. Except for the HSLA 340, all steels were tested at various temperatures by hot tensile testing (Refs. 11, 12). Data for the HSLA 340 steel are taken from the existing material database of the simulation software, SORPAS® (Ref. 13). The sheets were cut into samples of 25 × 100 mm (1 × 3.9 in.) and welded according to the setup shown in

Table 1 — Specification of Sheet Materials

Material	Supplier	Thickness [mm] (in.)	Coating [μm](μ in.)	Nominal composition [wt-%] C	Mn	Cr	Si	P	S	Al
DP600	SSAB	1.5 (0.059)	—	0.11	0.9	—	0.4	0.015	0.002	0.04
TRIP700	ThyssenKrupp	1.2 (0.047)	Zn: 14 (9/16)	0.24	2.0	0.6	0.3	0.4	0.01	0.24
HSLA 340	SSAB	0.8 (0.031)	—	0.05	0.40	—	0.01	0.01	0.01	0.04
DC06	SSAB	0.6 (0.024)	—	0.002	0.15	—	—	0.01	0.01	0.04

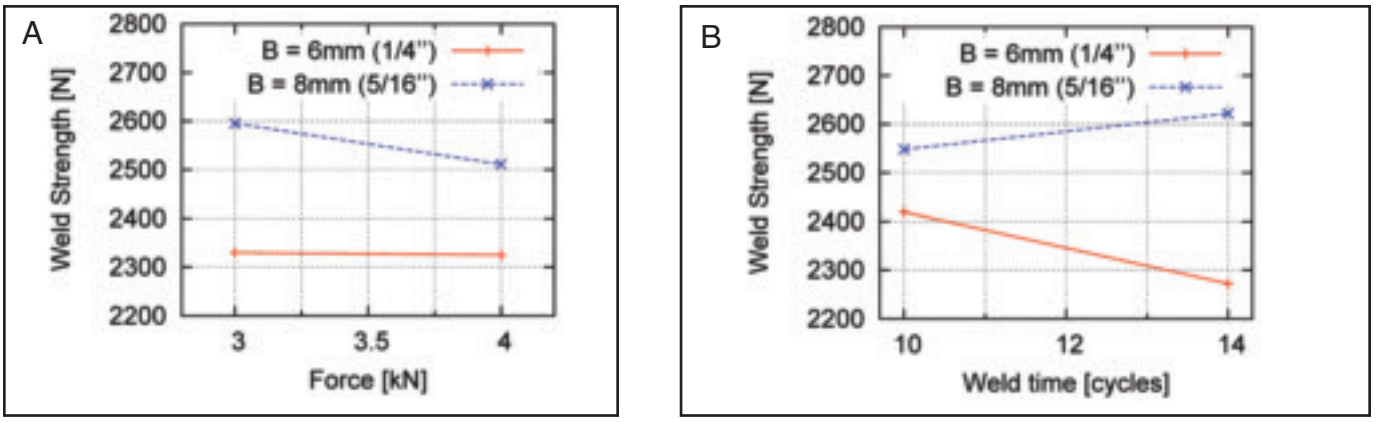

Fig. 3 — Plot of factor interactions for weld series 1; A — Electrode size and electrode force; B — electrode size and weld time.

Fig. 2. Reference code to a specific three sheet weld combination is abbreviated sheet1–sheet2–sheet3 as for instance DC06-HSLA 340-TRIP700, where the first-mentioned material is the top sheet. In all experiments the top sheet is the thin, low-carbon steel, while the two others vary.

The weld strength was tested in tension shear tests on a 100 kN (22.5 klbf) Amsler universal testing machine. The sheet samples were bent 20 deg prior to testing — Fig. 2. Prebending was applied in order to fit the samples into the available equipment in a way where a uniform test condition could be ensured. Testing was carried out by pulling the thin, low-carbon steel sheet apart from the two high-strength steels.

The influences of RMS current I, electrode force F, and weld time in cycles T on the weld strength were investigated. Furthermore, the effect of increasing tip diameter B of the bottom electrode from Ø6 mm (¼ in.) to Ø8 mm (5⁄16 in.) was studied. No up- or down-slope of the current or force were used.

The experimental investigations were designed as unreplicated 2^k full-factorial designs with $n_C = 3$ center points. This design was chosen in order to get an overview of the influence of the main parameters as well as possible interactions on the weld quality, i.e., failure type, strength, and splash/no splash. The center points were used to estimate the variability due to stochastic error in the experiments. The experiments were divided into seven series. The first three series investigated welding of DC06 to HSLA 340 as the middle sheet and either DP600 or TRIP700 as the bottom sheet. These series are named DC06-HSLA 340-DP600/TRIP700. The last four series investigated welding of DC06 to DP600 and TRIP700 in the four possible combinations. An overview of the factorial experiments is given in Table 2.

Series 1 and 2 were carried out as initial studies to test the overall weldability of DC06 to HSLA and AHSS. Furthermore, the influence of increasing the size of the bottom electrode was included in these series. Based on the first two series, the third series was carried out with identical process parameters for the two material combinations and using larger bottom electrode, Ø8 mm (5⁄16 in.) tip. Beside the factorial experimentation, series 3 was studied further to investigate nugget formation and weld strength over the entire current range at two force levels. The last four series, 4–7, were made to increase the complexity of the welding process even further by introducing AHSS next to the DC06 in different combinations while keeping the weld parameters the same for all combinations.

Performing the weld series 1–7, the weld current was entered on the control unit according to the values in Table 2. Measurements of the actual RMS weld current were used in the simulation instead of the prescribed values on the controller.

Numerical Procedure

The numerical software SORPAS® (Ref. 13) was used to simulate the process of three-layer spot welding. The software is a numerical tool specialized for resistance welding processes with simulation, optimization, and planning features. It is based on the finite element method, having a mechanical, thermal, electrical, and metallurgical model implemented. The three models are coupled in each time increment. Besides an existing material database, the software allows for material data provided by the user, such that specific materials can be simulated. The stress-strain curves for varying temperatures of the low-carbon steel, DC06, and the two high-strength steels, DP600 and TRIP700, were determined by hot tensile testing (Refs. 11, 12) and inserted in the

Table 2 — Overview of Factorial Designs

	Factor:	Current		Force		Time		Electrode		Material	
	Units:	[kA]		[kN]		[cycles]		[mm] (in.)			
Series	Factor abbreviation:	I		F		T		B		M	
No.	Three Sheet Combination	Low	High	Low	High	Low	High	Low	High	Low	High
1	DC06 HSLA 340 DP600	6.8	8.5	3	4	10	14	6(1/4)	8(5/16)	–	–
2	DC06 HSLA 340 TRIP700	5.1	6.8	3	4	8	12	6(1/4)	8(5/16)	–	–
3	DC06 HSLA 340 DP/TRIP	6.0	7.7	3	4	6	12	–	8(5/16)	TRIP	DP
4	DC06 TRIP700 TRIP700	6.8	8.5	3	4	12	20	–	8(5/16)	–	–
5	DC06 TRIP700 DP600	6.8	8.5	3	4	12	20	–	8(5/16)	–	–
6	DC06 DP600 TRIP700	6.8	8.5	3	4	12	20	–	8(5/16)	–	–
7	DC06 DP600 DP600	6.8	8.5	3	4	12	20	–	8(5/16)	–	–

software. The stress-strain-temperature curves for HSLA 340 as well as all thermal and electrical properties were taken from the existing material database of SORPAS®. In all simulations presented in this work, minimum two elements were used in the thickness direction of the sheets, and the time step was set to 0.2 ms.

Results

Weld Strength

In Table 3 the ANOVA tables of the reduced, fixed effects models for the experimental series 1 to 3 are collected employing specific procedures (Ref. 14). A relatively tight significance level of 2.5% was chosen in order to clarify only the most significant factors. Hence, factors with a significance level larger than 2.5% were dropped from the model and their sum of squares (SS) were pooled in the residual SS. The significance level (Prob. $> F_0$) for each significant factor (factor abbreviations are listed in Table 2) and factor interaction is listed in Table 3 together with the calculated sum of squares and its degree of freedom (DF). All factors only have two levels, and hence, all factors have one degree of freedom. The mean square is calculated and the ratio F_0 between factor mean square and the mean square of the total experimental variability, the residual, is calculated. Using the *F*-distribution, the null hypothesis is tested, and the probability that the variance in the experimental data is caused by stochastic error alone, and not by the variation of the factor levels, is calculated. A low probability implies that the factor or factor combination has a significant effect on the strength of the welds. The sum of squares of the residual consists partly of pure error calculated from the three center point repetitions and partly of the sum of squares from the insignificant factors that are dropped from the model. Finally, the overall mean weld strength and standard deviation are given as well as the values of the center point itself.

As an example on how the models were reduced using a significance level of 2.5%, the iteration of series 1 is shown in Table 4. It is seen from the table that the electrode force and weld time are close to being significant, which is expected, but in the reduced model of series 1 the main factor contributing significantly to increasing the weld strength is the electrode size *B*, and the main interactions are between electrode size and force *BF* as well as electrode size and weld time *BT*. The two significant interactions are shown in Fig. 3. Had the parameter range been chosen differently (i.e., lowering the minimum values), the main parameters *F*, *T*, and *I* would most likely have had a significant effect. The fact that different factors have an effect depending on the chosen parameter range can be attributed to the experimental variation and errors introduced by the linearity assumption of the 2-level factorial design.

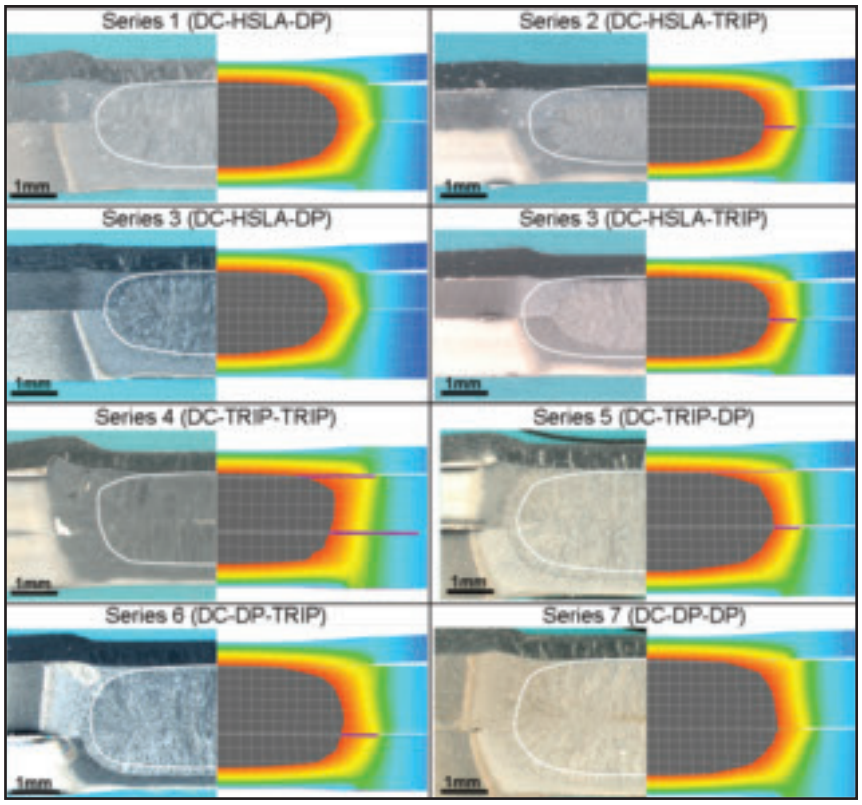

Fig. 4 — Experimental and numerically calculated cross-sectional views of center-point welds in weld series 1 through 7.

In series 1, where DC06-HSLA 340-DP600 is the weld combination, it is seen how increasing weld time decreases strength using the small electrode, while the strength is increased if using a larger bottom electrode — Fig. 3B. This is attributed to the fact that the small electrode promotes splash at longer weld time, while the larger electrode allows for the growth of a larger nugget resulting in higher strength. The force has no effect on the weld strength using the small electrode, while the strength decreases when increasing the load with the large bottom electrode — Fig. 3A. This is explained by considering the relation between pressure and contact resistance. Using the small electrode, the pressure is higher compared to the large electrode, and for high pressures the effect on contact resistance and heat generation levels out. Furthermore, increasing electrode size alone raises the strength — Fig. 3. The current shows no influence on weld strength. This is most likely because the actual current values in the experiments were considerably lower and lying closer to each other (<1 kA) than prescribed on the controller. On top of this, the nugget size becomes more robust in regard to weld current when approaching the splash limit, which is the case here.

Series 2 involves welding of DC06-HSLA 340-TRIP700, where different weld parameter settings than the previous are used (Table 2). In the ANOVA analysis of series 2, the current *I*, force *F*, and weld time *T* now have significant effects on the weld strength, while on the other hand, the electrode size *B* does not have an effect. The fact that *I*, *F*, and *T* influences are significant suggests that the ranges of the factor levels are wide enough to cover the nugget growth. For higher levels of these factors, their effect on nugget size and strength saturates, thereby becoming insignificant. For this material combination, the weld strength did not increase when increasing the size of the bottom electrode. This could suggest that the nugget is not allowed to grow to its potentially full size and the effect of a smaller pressure due to the larger electrode drowns in the main effect of changing the actual load itself. This is supported by the fact that the average weld strength of the center points for series 2 is noticeably lower than for series 1 when considering the standard deviation of the results. This suggests that the nugget in series 2 could still be allowed to grow to obtain a larger nugget and, thereby, higher strength.

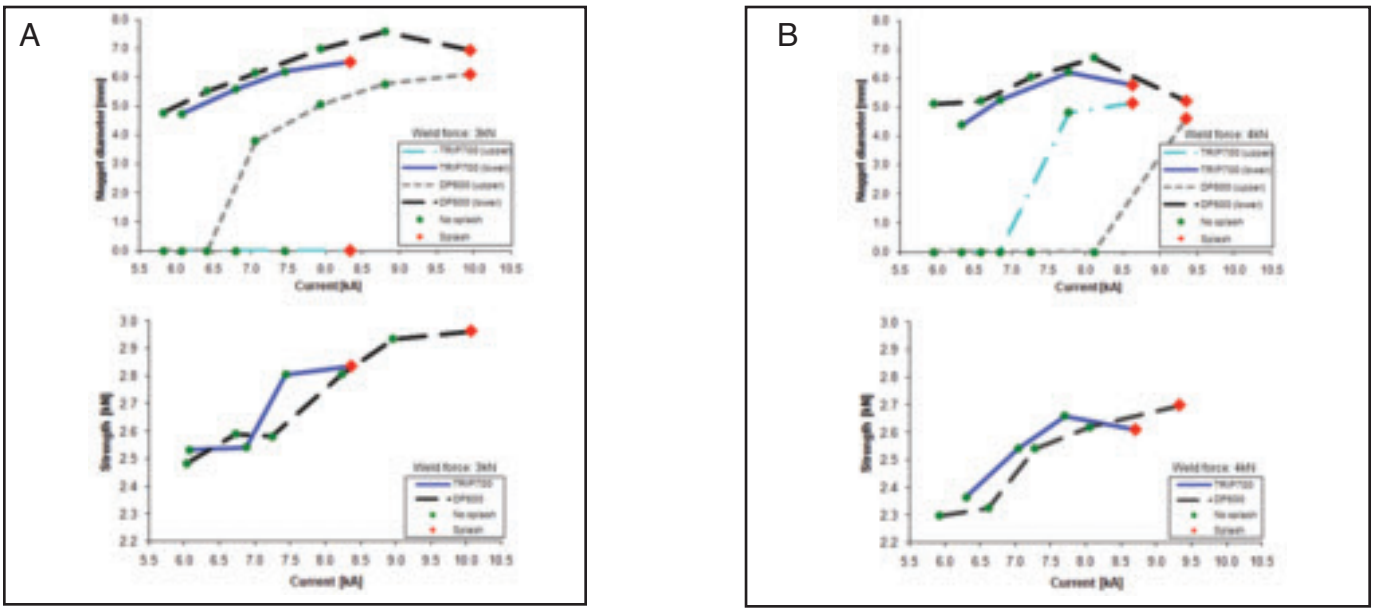

Fig. 5 — Upper: Nugget diameter at upper interface (DC06-HSLA 340) and lower interface (HSLA 340-TRIP700/DP600) for varying weld current at two weld force levels; A — 3 kN; B — 4 kN. Lower: Corresponding weld strengths.

Due to the fact that increasing the size of the bottom electrode promoted higher strength and eliminated splash in series 1 as well as having no effect in series 2, it was chosen to apply the larger size bottom electrode with tip Ø8 mm (5/16 in.) in the remaining series 3–7, which were then focused on the effect of the material combinations.

Series 3 was run with a large lower electrode and common factor levels for the two material combinations: DC06–HSLA 340–TRIP700/DP600. The factor level ranges were set to overlap the ranges of the two previous series, hereby increasing the average heat input when using the TRIP steel and decreasing the average heat input when using the DP steel. The ANOVA analysis (Table 3) suggests that the factors material *M*, current *I*, force *F*, and weld time *T* all have significant effects on the weld strength. Changing the material from TRIP to DP or increasing the electrode force decreases the average weld strength, while an increase in current and weld time increases weld strength. At the high heat input settings for the TRIP combination, splash starts being a problem, although the weld strength is not negatively influenced by this. Since no interactions involving the material type of the bottom sheet are significant, the factors *I*, *F*, and *T* have the same effects on the relative weld strength independent of material type. This suggests that the lower absolute values of the factor level range for

Table 3 — ANOVA Tables of Series 1 to 3

Series 1: DC06 – HSLA340 – DP600

Factor	Sum of Squares	DF	MS	F_0	Prob. > F_0	Weld Strength	Overall	Center Point
B	228711.1	1	228711.1	63.2	<0.00%	Mean [N] (lbf)	2488 (559.3)	2611 (587.0)
BF	32052.64	1	32052.6	8.9	1.07%	Std. Dev. [N] (lbf)	151 (33.9)	12 (2.7)
BT	48719.53	1	48719.5	13.5	0.28%			
Residual	47027.37	13	3617.5					

Series 2: DC06 – HSLA340 – TRIP700

Factor	Sum of Squares	DF	MS	F_0	Prob. > F_0	Weld Strength	Overall	Center Point
F	39951.5	1	39951.5	46.1	<0.00%	Mean [N] (lbf)	2434 (547.2)	2403 (540.2)
T	58356.7	1	58356.7	67.4	<0.00%	Std. Dev. [N] (lbf)	108 (24.3)	29 (6.5)
I	83041.2	1	83041.2	95.9	<0.00%			
Residual	20839.6	13	1603.0					

Series 3: DC06 – HSLA340 – DP600/TRIP700

Factor	Sum of Squares	DF	MS	F_0	Prob. > F_0			Center Point	
M	29052.8	1	29052.8	9.5	0.80%	Weld Strength	Overall	DP	TRIP
F	30748.9	1	30748.9	10.1	0.67%	Mean [N]	2594 (583.2)	2606 (585.9)	2672 (600.7)
T	56010.9	1	56010.9	18.4	0.07%	Std. Dev. [N] (lbf)	107 (24.1)	25 (5.6)	44 (9.9)
I	59547.6	1	59547.6	19.6	0.06%				
Residual	42631.6	14	3045.1						

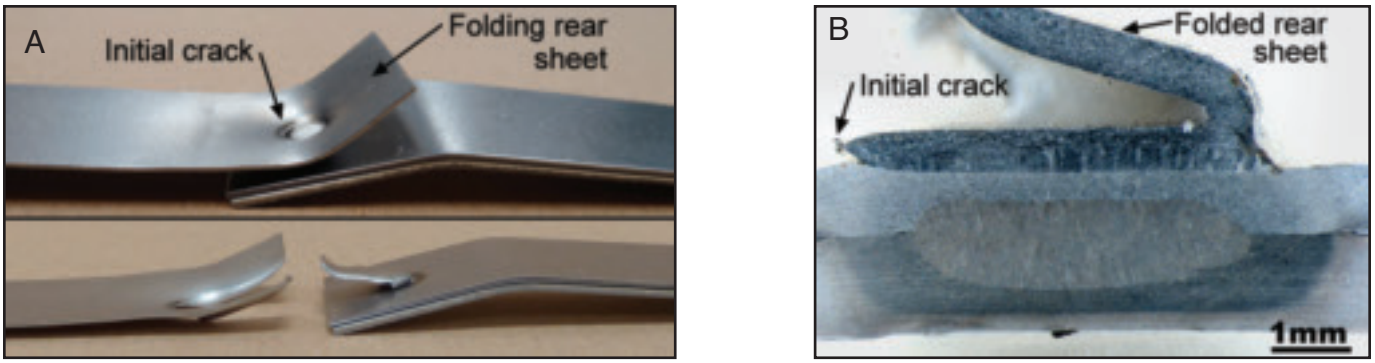

Fig. 6 — Weld combination DC06-HSLA 340-TRIP700 welded with 6.3 kA during 16 weld cycles at 4 kN weld force. Upper A — Initial crack formation after maximum load. The rear of the thin sheet has started folding. Lower A — Complete separation showing a plug failure with subsequent tearing of the thin sheet, which is now folded over the remaining button; B — cross section showing the plug failure and nugget, which has not formed into the thin, low-carbon sheet.

DP steel covers more of the nugget growth region than in series 1. The strength is, therefore, now influenced by these factors. The standard deviations of the center runs indicate that the TRIP steel gives higher variability than the DP steel.

Series 4–7 were all carried out with the large bottom electrode tip of Ø8 mm (5/16 in.). Analysis of the results from the factorial experiments using the ANOVA procedure presented some problems. This is mainly due to the fact that the ANOVA analysis works best with process responses that are continuous. When a certain parameter configuration yields no weld, the recorded weld strength is zero, which gives a large discontinuous jump in the response. Furthermore, some of the welds resulted in an abnormally high indentation of the top electrode, which resulted in a highly increased nugget size and again a jump in weld strength. These jumps will corrupt the ANOVA analysis and either show large effects from factors that are not expected to be significant, or show no effect due to a too high variability in the results. In Table 5, the results of the different series are collected showing the overall and center point averages and standard deviations. The overall averages and standard deviations for series 4–6, all including the TRIP steel, show large variability in the chosen range of the factor levels, meaning that changing the process parameters causes a large change in response of the process. Comparing with the standard deviations of the center points, it is clear that the main process parameters highly affect the results of these welds.

The DC06-TRIP700-TRIP700 combination showed splash at high heat input settings and practically no welds at low heat input. Furthermore, splash was also observed for one of the low heat input settings indicating that the TRIP sheet itself is inducing variability to the process. This is also seen from the relatively large standard deviation of the center point runs and the fact that splash was not consistent for the repeated center point runs.

Introducing the DP steel drastically changed the results, and the effect was highly dependent on the order of the materials in the three layers. In the DC06-TRIP700-DP600 combination (series 5), the factorial experiments resulted in an even larger variability. This was due to the fact that some of the weld configurations produced no joint between the DC06 and the TRIP700 while others resulted in splash and high strength. The center points show that the strength is much lower compared to the other combinations, and the failure mode is weld interface failure. If, on the other hand, the DP600 is inserted next to the DC06 steel in the DC06-DP600-TRIP700 combination (series 6), the average weld strength increases, and the process becomes much more robust strength-wise with successful welds at all factor level combinations, although with significant amount of splash at low force settings (3 kN). In series 7, the TRIP steel has been replaced by DP steel implying the material combination DC06-

Table 4 — Iteration Scheme Using the 2.5% Significance Level to Drop Factors from the Model

	Iteration 1			Iteration 2			Iteration 3		
Factor	DF	Ms	P	DF	MS	P	DF	MS	P
B	1	228711.1	0.07%	1	228711.1	0.00%	1	228711.1	0.00%
F	1	13286.6	1.13%	1	13286.6	2.88%	–	–	–
T	1	5413.3	2.70%	–	–	–	–	–	–
I	1	1178.9	10.86%	–	–	–	–	–	–
BF	1	32052.6	0.47%	1	32052.6	0.25%	1	32052.6	1.07%
BT	1	48719.5	0.31%	1	48719.5	0.05%	1	48719.5	0.28%
BI	1	10610.0	1.41%	1	10610.0	4.62%	–	–	–
FT	1	4066.0	3.55%	–	–	–	–	–	–
FI	1	1178.9	10.86%	–	–	–	–	–	–
TI	1	2652.5	5.29%	–	–	–	–	–	–
BFT	1	5413.3	2.70%	–	–	–	–	–	–
BFI	1	216.5	35.55%	–	–	–	–	–	–
FTI	1	1353.3	9.66%	–	–	–	–	–	–
BFTI	1	1353.3	9.66%	–	–	–	–	–	–
Pure Err.	2	152.4		2	152.4		2	152.4	
Lack of Fit	4	8336.5		9	2536.2		11	4248.5	
Residual	6	8488.9		11	2102.8		13	3617.5	

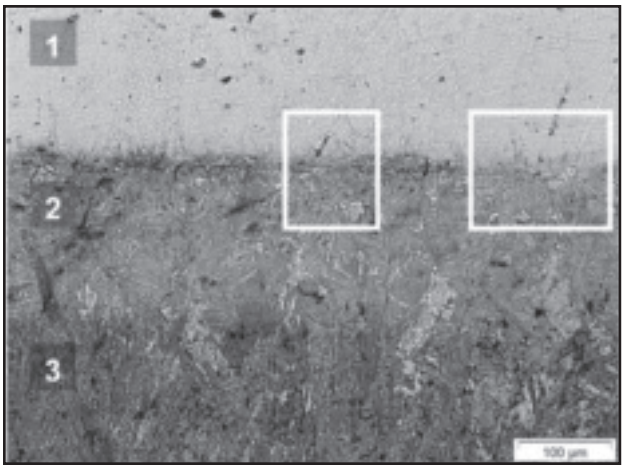

Fig. 7 — DC06-HSLA 340 interface in welds series 2.

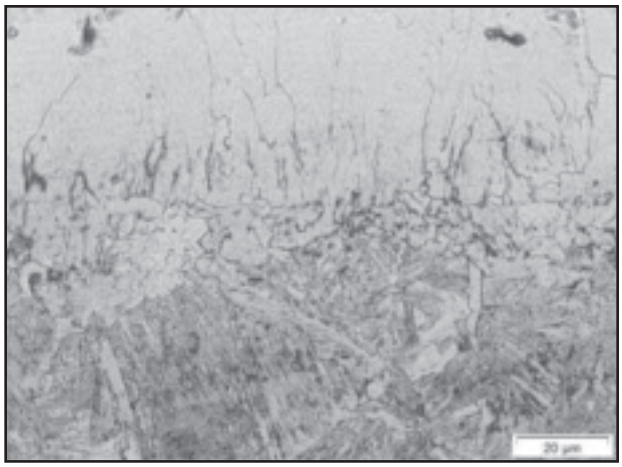

Fig. 8 — Area of bonded interface, series 2.

DP600-DP600. This combination is extremely robust in the chosen parameter range as the weld strength hardly changes and no splash is observed. An ANOVA analysis on this series suggests that only the current has notable influence and that the effect is small.

The experimental investigation of weld strength shows that the zinc-coated TRIP steel makes the process more sensitive to process variations. When including this sheet in the combination, the process window for making a successful weld diminished. The dominant failure mode during tension shear testing was identified as plug failure and subsequent tearing of the thin low-carbon steel sheet.

Nugget Formation

The nugget formation mechanism in three-layer welding of a low-carbon sheet to two high-strength steels was investigated using numerical simulation of the process. The simulations give the temperature distribution in the material at a given time during the process. An analysis of temperature development during welding revealed that for the present configuration of materials and sheet thicknesses, the heat generation was concentrated around the interface between the two thicker high-strength steels, which was the location of initial nugget formation. Depending on the material combination and the thickness of the sheets, the weld nuggets grow toward the interface to the thin, low-carbon steel. Conventionally, the optimal weld is achieved if the nugget is allowed to grow a considerable amount into all the sheets being joined. However, the problems regarding the investigated three-sheet welds were to achieve nugget growth into the thin low-carbon steel sheet without getting splash and internal defects in the weld.

Looking at the cross-section micrographs of the center-point runs of series 1 through 7(Fig. 4), it is seen how the resulting weld nuggets appear. The simulated temperature distribution and weld nuggets are shown for comparison; the white line drawn in the micrograph showing the predicted nugget. The micrographs indicate that the nugget has not been able to grow into the thin, low-carbon steel sheet in any of the weld series' center point runs. The nuggets tend to grow close to the interface of the low-carbon sheet, but then it stops, in some cases practically at the interface. For other weld configurations than the center-point settings, the nugget penetrates slightly into the low-carbon steel.

From the simulations, it is furthermore observed that the weld nugget generation is strongly influenced by the presence of the zinc coating on the TRIP steel. According to the simulations, the initiation of the weld nugget formation is delayed due to the improved contact conditions in the interface and the resulting reduced heat generation. The simulations suggest that the nugget formation initiates in the bulk part of the sheets rather than at the interface, but then almost immediately after grows through the interface forming a weld nugget between the two high-strength steels. In general, rather good agreement between simulated and experimentally obtained nugget sizes is observed — Fig. 4. The largest discrepancy is noticed in weld series 3 when introducing the TRIP steel, where the simulated nugget size is somewhat larger than the experimentally obtained. This was likely caused by the modeling of the contact resistance at the two zinc-coated surfaces of the TRIP steel, where the simulated heat generation and the squeeze out of the liquid coating is overestimated compared to the real situation.

A detailed study of the nugget growth and resulting strength was carried out for series 3. The resulting nuggets for the two material combinations, DC06-HSLA 340-

Table 5 — Results of the Factorial Experimental Series 4 to 7

No.	DC06 –	Overall Average [N] (Ibf)	Overall Std. Dev. [N] (Ibf)	Center Point Average [N] (Ibf)	Center Point Std. Dev [N] (Ibf)	Failure mode of center point	Center point weld splash
4	TRIP-TRIP	2169 (487.6)	973 (218.7)	2706 (608.3)	155 (34.8)	Tearing of base metal	Splash
5	TRIP-DP	1867 (419.7)	1467 (329.8)	2011 (452.1)	121 (27.2)	Weld interface failure	No splash
6	DP-TRIP	3062 (699.4)	632. (142.1)	2904 (652.8)	103 (23.2)	Tearing of base metal	No splash
7	DP-DP	2836 (637.6)	91 (20.5)	2830 (636.2)	25 (5.6)	Tearing of base metal	No Splash

TRIP700/DP600, were examined for different current settings. The current was varied from the minimum setting on the machine (about 6 kA) in steps until splash was reached. The welding time was increased to 16 cycles to increase possibility of nugget growth into the thin, low-carbon sheet. The two force levels were kept at 3 and 4 kN. Figure 5 shows the nugget diameters at the two interfaces as well as the obtained strength for the four combinations (two material combinations and two weld force levels). In agreement with previous discussion, the combination including the coated TRIP steel has a narrower weldability range. Splash is reached at lower currents, and the nugget growth at the DC06-HSLA 340 interface (referred to as upper interface in Fig. 5) is more difficult to achieve. At 3 kN weld force for the TRIP combination, no nugget was formed before splash appears, whereas the DP combination has a relatively large current range at 3 kN, where a nugget forms into the thin DC06 sheet. The corresponding strengths are shown by Fig. 5 (lower). As all points in Fig. 5 are unreplicated, an idea of the standard deviation is obtained by comparing with the center runs for series 3 (Table 3). As the weld settings are changed, a larger deviation is assumed in order to be conservative. Reading the strength curves in Fig. 5 as ± 0.1 kN corresponds to ± 2.3 times the maximum standard deviation obtained in the original series 3. Having this in mind, a general trend is increasing strength with increasing current as the nugget also increases by increasing heat input.

An interesting discovery from the strength tests is that all tested welds failed with plug failure and subsequent tearing of the thin, low-carbon sheet. This being regardless of whether or not nugget formation appears in the DC06-HSLA 340 interface. Figure 6 shows an example of a weld without nugget formation into the thin sheet, but with plug failure. The example is a DC06-HSLA 340-TRIP700 combination welded with 6.3 kA during 16 cycles using a weld force of 4 kN. The upper part of Fig. 6A shows the initial crack and the rear sheet starting to fold. The lower part of Fig. 6A shows the configuration after complete separation. A button has formed from the thin sheet, and the thin sheet behind the button has been torn apart from the remaining thin sheet. Figure 6B shows the button on top of the two high-strength steels, and it shows the nugget, which has only penetrated roughly half through the HSLA 340 sheet, thus not forming a nugget in the critical interface to the thin low-carbon sheet. The strong bond between the low-carbon steel and the neighboring high-strength steel is a solid-state bond facilitated by heat and plastic deformation.

Bonding Mechanism

The tension shear tests resulted in a rather high strength of the joints compared to previous studies (Ref. 3) as well as plug failure followed by ductile fracture of the low-carbon steel in most cases, although in some cases, the nugget only penetrated slightly or not at all into the thin, low-carbon sheet. This implies that the low-carbon steel is effectively joined to the high-strength steels. A closer inspection of the micrographs revealed several different weld interfaces between the low-carbon and high-strength steel.

Contaminant film and oxide layers are broken by heating and plastic deformation uncovering virgin metal surfaces, which leads to direct metal-to-metal contact and formation of a strong metallic bond, i.e., a solid-state joint. In some cases the entire interface is bonded, while less favorable bonding conditions only allow for parts of the interface to form strong bonds. This is seen in Fig. 7 showing the interface between low-carbon steel and HSLA in weld series 2. Outside the boxed areas, the original interface is still intact and visible as a black line separating the two steels. Inside the boxes, the interfaces have grown together, and the interface line is no longer present as seen in the magnification — Fig. 8. The larger bonding area, the higher is the expected tension shear strength of the welds. Three different material zones are distinguished in Fig. 7. Zone 1 consists of the low-carbon steel, zone 3 is the weld nugget now transformed into martensite, and zone 2 is the heat-affected zone of the HSLA in contact with the low-carbon steel. With reference to the tension shear strength of the center point run of weld series 2 given in Table 3, it is clear that a strong bond is created even though the weld nugget clearly has not reached the joining interface.

Discussion

From the factorial experimental series 1 and 2, it is shown that increasing the tip diameter of the bottom electrode from Ø6 mm (¼ in.) to Ø8 mm (5/16 in.) significantly increases the tension shear strength of the weld combinations with DP600, but not with TRIP700. As proposed in section 3.1, the main reason for this is that the maximum nugget size had been reached using the small electrode and a larger electrode allows for the growth of a larger nugget. The process parameter range of the TRIP700 was not chosen as close to the maximum nugget size, and hence, an increased electrode size could not generate a larger nugget for the chosen weld parameters. On the other hand, it is noticed that a change in process parameters gave stronger welds and presumably larger weld nuggets.

As seen from the factorial experiments, especially series 4–7, the three-layer welding generally becomes less robust toward changes in process variables when the coated TRIP steel is included in the material combination. Comparing the tensile properties (Fig. 1), it is seen that the TRIP steel itself is stronger than the DP steel. However, it is the tensile properties of the DC06 that is most important for the strength when the failure mode is plug failure. A numerical simulation, where the material properties of DP600 in weld series 3 were replaced by the properties of TRIP700, showed that the difference in nugget diameter was less than 4%. Thus, the effect of the different mechanical properties of the TRIP and DP is limited. The electrical properties of the bulk materials are furthermore not differing significantly since all the materials are steel alloys with relatively low amounts of alloying elements. The fact that the TRIP steel is thinner than the DP steel affects the welding process, as the cooling capacity of the sheet itself is decreased, but on the other hand the interfaces move closer to the electrodes, thereby facilitating cooling.

The main factor influencing the weldability of the TRIP steel is believed to be the 14 μm (5/16 μin.) zinc coating, as also the influence of coating on low-carbon steels has been shown previously (Ref. 8). The coating is soft and a good electrical conductor resulting in low contact resistance of the interfaces and slower heat generation, thereby delaying the nugget formation, in agreement with the previous measurements and discussions (Ref. 8). This implies that longer weld times or higher currents are needed to initiate nugget growth. As the melting point of zinc is considerably lower than that of the steels, the coating melts before the nugget forms at a given interface. Due to the high contact pressure, the melted coating will be squeezed out. The coating only stays at an interface in cases where the temperature stays below the melting temperature of the coating. In practice, this implies that whenever a nugget forms at a zinc-coated interface, the coating has been squeezed out.

After the coating has been squeezed out, the molten zinc will segregate in the periphery of the nugget, thereby increasing the contact area. This increased contact area counteracts the increased contact resistance in the area that the coating has left. In the previous work (Ref. 8), a larger welding current was applied for the coated case than for the uncoated case. In this case, similar nugget growth rates were obtained for the two cases, since the larger welding current compensated for the

larger contact area. A numerical study of series 3, using SORPAS® (Ref. 13), showed that the nugget diameter increased by more than 23% when removing the zinc coating in the HSLA 340-TRIP700 interface under the same welding parameters. This is in agreement with the choice in Ref. 8, where the optimal welding current was found to be larger in the coated case.

Conclusions

The mechanism of nugget formation has been identified to initiate between the two high-strength steels from where it develops and grows into the sheets. Depending on the heat input, the nugget might grow close to or in some cases even slightly penetrate into the thin, low-carbon steel. It was found that increasing the size of the bottom electrode improved the strength of the joints by increasing the weld nugget diameter. This, however, was only observed for weld settings where the growth of the nugget was restricted not due to a low heat input but to geometrical concentration of the current, i.e., in cases where the weld current and time were enough to form a nugget of at least the size of the bottom electrode tip.

By examining micrographs of the welds, it was found that bonding between the low-carbon steel and high-strength steels predominantly appeared in solid state rather than by a fusion nugget. The solid-state bonding is facilitated by the high temperatures and plastic deformation during the welding process breaking the oxide layer to form metallic bonds. The weld strengths measured by tension shear tests were found to be relatively high compared with previous investigations utilizing the same low-carbon steel (Ref. 3). Furthermore, fracture was typically in the form of ductile tearing of the low-carbon steel around the formed plug failure. Only a few of the weaker welds failed in a brittle manner through the interface, and this was mainly observed for interfaces with zinc coating involved, i.e., for the TRIP steel.

It was investigated whether it was possible to model the three-layer welding process by numerical simulation using material models of the strength of the materials determined by hot tensile testing. The simulations proved good correlation with the experimental results, which shows that the numerical analysis can be used as a tool to optimize individual weld configurations of three-layer spot welding of AHSS.

As mentioned in the introduction, lack of confidence in weld quality for three-sheet spot welding results in many more welds than needed for the required structural performance (Ref. 8). Another reason for applying too many welds could be incorrect quality measures. Nugget size has traditionally been a quality measure, but the results obtained in the present work show that a satisfactory high strength involving plug failure can be achieved even without forming a fusion zone across the interface to the thin, low-carbon steel in typical three-layer welds. Increased confidence in such welds, e.g., obtained by performing additional types of strength, fatigue, or impact tests, may lead to fewer welds if a larger span of welds can be accepted.

Acknowledgments

The second author is indebted to assistance by Professor Paolo Bariani and Dr. Stefania Bruschi at DIMEG, University of Padova, where he carried out the hot tensile tests. Furthermore, B.Sc. Mikael Kjeldal Jensen is acknowledged for his large experimental contribution. The present project is part of the INNOJoint project supported by the Danish Council for Independent Research, Technology, and Production Sciences. The companies SSAB and ThyssenKrupp are acknowledged for supplying the steel materials.

References

1. Khan, M. I., Kuntz, M. L., and Zhou, Y. 2008. Effects of weld microstructure on static and impact performance of resistance spot welded joints in advanced high strength steels. *Science and Technology of Welding and Joining* 13(1): 49–59.

2. Uijl, N., and Smith, S. 2006. Resistance spot welding of advanced high strength steel for the automotive industry. *Proceedings of the 4th International Seminar on Advances in Resistance Welding*, pp. 30–62.

3. Pedersen, K. R., Harthøj, A., and Friis, K. L. 2008. Microstructure and hardness distribution of resistance welded advanced high strength steels. *Proceedings of the 5th International Seminar on Advances in Resistance Welding*, pp. 134–146.

4. Hernandez, V. H. B., Kuntz, M. L., and Khan, M. I. 2008. Influence of microstructure and weld size on the mechanical behaviour of dissimilar AHSS resistance spot welds. *Science and Technology of Welding and Joining* 13(8): 769–776.

5. Bohr, J., Jiang, C., and Sang, Y. 2008. Resistance spot welding of advanced high strength steel, a comparative study of joint efficiency. *Proceedings of the 5th International Seminar on Advances in Resistance Welding*, pp. 147–166.

6. Zhang, Y. S., Sun, H. T., Chen, G. L., and Lai, X. M. 2009. Comparison of mechanical properties and microstructure of weld nugget between weld-bonded and spot-welded dual-phase steel. *Proceedings of the Institution of Mechanical Engineers, Part B: Journal of Engineering Manufacture* 223(10): 1341–1350.

7. Schreiber, S. 2001. Investigations into three-member welding (in German). *Schweissen und Schneiden/Welding and Cutting* 53(11): 574–585.

8. Harlin, N., Jones, T. B., and Parker, J. D. 2003. Weld growth mechanism of resistance spot welds in zinc coated steel. *Journal of Materials Processing Technology* 143–144: 448–453.

9. Ikeda, R., Okita, Y., and Ono, M. 2008. Development of new resistance spot welding process for three sheet joints using electrode force control. *Proceedings of the 5th International Seminar on Advances in Resistance Welding*, pp. 105–113.

10. Fronius International GmbH. DeltaSpot. Retrieved June 24, 2010, from *www.fronius.com/cps/rde/xchg/fronius_usa/hs.xsl/3022_2888.htm*.

11. Bariani, P. F., Bruschi, S., and Ghiotti, A. 2008. Testing formability in the hot stamping of HSS. *Cirp Annals-Manufacturing Technology* 57(1): 265–268.

12. Friis, K. S. 2010. Resistance welding of advanced materials and micro components. PhD thesis, Technical University of Denmark.

13. SORPAS®, Version 10, SWANTEC Software and Engineering ApS.

14. Montgomery, D. C. 2005. *Design and Analysis of Experiments*. John Wiley and Sons.

Authors: Submit Research Papers Online

Peer review of research papers is now managed through an online system using Editorial Manager software. Papers can be submitted into the system directly from the Welding Journal page on the AWS Web site (www.aws.org) by clicking on "submit papers." You can also access the new site directly at www.editorialmanager.com/wj/. Follow the instructions to register or login, and make sure your information is up to date. This online system streamlines the review process, and makes it easier to submit papers and track their progress.